PR11 Studies on Actinides and Fission Products Performed at the KURRI Hot Laboratory

T. Fujii

Research Reactor Institute, Kyoto University

1. Objectives and Allotted Research Subjects

Studies on actinide and fission product nuclides with careful management are being more important for reprocessing, disposal, partitioning, and transmutation processes in the nuclear fuel cycle. Hot laboratory of KURRI is one of core facilities in Japan, in which various nuclides can be handled. This project enhances utilization of the KURRI hot laboratory by opening for fundamental and application studies related to radiochemistry, nuclear chemistry, environmental chemistry, geochemistry, and so on. Allotted research subjects are;

ARS-1 Complexation of actinides with organic substances (T. Sasaki *et al*.).

ARS-2 Solubility of actinide compounds in aqueous media (T. Kobayashi *et al*.).

ARS-3 Leaching of actinides and FPs from fuel debris (N. Sato *et al*.).

ARS-4 Neutron irradiation damage of vitrified waste matrices (T. Nagai *et al*.).

ARS-5 Ligand exchange reaction of actinides in molten salts (A. Uehara *et al*.).

ARS-6 Electrochemical behavior of uranium in pyroreprocessing system (Y. Sakamura *et al.*).

ARS-7 Structural study of f-elements in molten halides (H. Matsuura *et al*.).

ARS-8 Molecular dynamics simulation of uranyl ion in molten salts (N. Ohtori *et al*.).

ARS-9 Fundamental study of fission products for trans-actinide chemistry (Y. Kasamatsu *et al*.).

ARS-10 Isotope separation by using microreactor (R. Hazama *et al*.).

ARS-11 Optical properties of molten aluminum halides (T. Goto *et al*.).

ARS-12 Precipitation of f-element oxides in molten halides (H. Sekimoto *et al*.).

ARS-13 Uptake of radiocesium and radiopotassium in plants (T. Ohta *et al*.).

ARS-14 Quantitative analysis of radionuclides in seawater (T. Kubota *et al*.).

ARS-15 Isotopic composition of radionuclides in environmental samples (Y. Shibahara *et al*.).

ARS-16 Noble gas mass spectrometry of neutron irradiated geological samples (H. Sumino *et al*.).

ARS-17 $^{40}Ar/^{39}Ar$ dating of neutron irradiated minerals and glasses (O. Ishizuka *et al*).

ARS-18 Radiometric Ar-Ar dating of neutron irradiated lavas (N. Hirano *et al*.).

2. Main Results and Contents

ARS-1, 2, 3, and 4 were performed in order to deepen the knowledge of nuclear waste management issues. In ARS-1 and 2, stability constants and solubility products of actinides were obtained. In ARS-3, leaching kinetics of actinides and FPs from irradiated Zr alloy was clarified. In ARS-4, a structural change of borosilicate by neutron irradiation was found. ARS-5, 6, 7, and 8 were performed with the viewpoint of pyroreprocessing. In ARS-5 and 7, ligand exchange of F^- and Cl^- for U^{4+} and Nd^{3+} in molten halides was clarified. In ARS-6, effective diffusion coefficient of U^{3+} in porous Zr was determined. In ARS-8, atomic distances of UO^{2+} in LiCl melt were computed. Polarization of Cl^- around UO_2^{2+} was found. ARS-11 and 12 seek applications of molten salt systems for industrial use, for example, refining. ARS-11 studied optical properties of molten alkaline chlorides containing Al. Raman spectra obtained were interpreted by using *ab initio* method. ARS-12 focuses on recycling of rare earths. Solubility of Dy(III) under the coexistence of Dy oxide and oxychloride in chloride melts was discussed. ARS-10 studied isotope fractionation of Ca. A possible fractionation of $^{48}Ca/^{40}Ca$ was found. ARS-13, 14, and 15 studied on redionuclides in soils, plants, seawater, and so on. In ARS-13, distribution of radiocesium in plants was clarified. ARS-14 presented an effective preparation method of radiotracers which are useful for environmental science. ARS-15 suggested that precise isotopic analysis of Cs and Sr is helpful for a rapid source analysis of nuclear accident. ARS-16, 17, and 18 demonstrated that neutron irradiation at KUR is usable for the Ar-Ar and I-Xe dating of geological samples.

3. Summaries of the achievements

In this research, by using various unique facilities of KURRI for actinides and fission products, new and characteristic chemical, kinetic, structural, and thermodynamic data were obtained. These new information encompass solid chemistry, molten salt and solution chemistry, as well as nuclear reactions of f-elements and FPs. The results are useful either for scientific purpose or for technological purpose for nuclear science, environmental science, geoscience, and general industry.

採択課題番号　26P11　ホットラボラトリを活用したアクチニドおよび核分裂生成物元素の化学研究　　プロジェクト

（京大・原子炉）藤井俊行

PR11-1 Apparent Formation Constant of Metal Ions with Humic Substances; Modelling

T. Sasaki, T. Kobayashi, T. Koukami, A. Uehara[1], T. Fujii[1], H. Yamana[1], H. Moriyama[1]

Graduate School of Engineering, Kyoto University
[1]Research Reactor Institute, Kyoto University

INTRODUCTION:
A semi-empirical thermodynamic model was developed to estimate the apparent formation constants of metal ions with humic substances (HSs), humic and fulvic acids, over a wide range of solution conditions, i.e., pH, ionic strength, and HS and metal concentrations.

To understand the fundamental rules of metal complexation with HSs, many researchers have attempted to characterize the physical and chemical properties of HSs in soils, sediments, and natural waters. It has been determined that randomly cross-linked heterogeneous organic substances generally have similar distributions of a number of specific functional groups, including carboxyl, phenolic, and alcoholic groups. Towards the ultimate goal of characterizing natural HSs, researchers have proposed hypothetical HS chemical structures based on results obtained using several analytical methods.

The discrete fragment model has been proposed by our group; it decomposes the organic ligands into discrete fragments of functional groups and chelating bridges that connect the functional groups. The ligand fragments called as basic ligands were clipped from a “pragmatic” chemical structure of a humic acid (HA) proposed [1], which were distributed statistically in the HA framework. The fixed formation constant values of the metal ion with each ligand was taken from the literature; benzoic acid, phthalic acid, isophthalic acid, 1,2,3-benzenetricarboxylic acid, 1,2,4-benzenetricarboxylic acid, 2-hydroxybenzoic acid, phenol, butanedioic acid, and acetic acid. The steric effect of bidentate binding sites due to the additional stabilization by chelate formation was considered, while the electrostatic surface potential of the HA molecule in solution was not considered for simplification. The model has yielded satisfactory results for the apparent complex formation constant of trivalent europium with Aldrich HA under varied solution conditions, including pH, ionic strength, and the concentrations of metal ions and HA [2].

THEORETICAL:
The model was modified and applied to several kinds of metal ions including actinides, i.e., Th(IV), Pu(IV), and Np(V), according to following steps; 1) a number of datasets for acid dissociation of various HSs were analyzed to obtain the representative values for the abundance ratios of the basic ligands and the heterogeneity parameter of HSs, 2) the datasets for complexation of various multivalent metal ions with HSs were analyzed to obtain the representative values for the intramolecular chelating effect of the bidentate site fraction. In the case of tetravalent metal ions, the hydrolysis reactions are taken into account for the analysis of the experimental datasets [3].

RESULTS:
The present model fairly well reproduced the literature apparent formation constants of tetravalent Pu/Th (Fig.1), pentavalent Np, divalent Ca/Co, and trivalent Al/Eu with the hypothetical humic acid and of tetravalent Th, pentavalent Np, divalent Mg/Ca/Co/Mn/Ni/Cu/Zn/Pb, and trivalent Eu with the hypothetical fulvic acid under a wide range of pH, *I*, and initial HSs and metal concentration [3]. Some discrepancies between the calculated and experimental values were recognized and discussed; one is the *I* dependence of the values of some metal ions such as neptunium, and the other is the discrepancy observed for the system of ultra-trace amount of neptunium, suggesting further effects of not yet identified but much stronger binding sites in HS. Although the present hypothetical structure is only one example of HS, it provides a basis for further studies of the thermodynamic and kinetic parameters for complexation reactions.

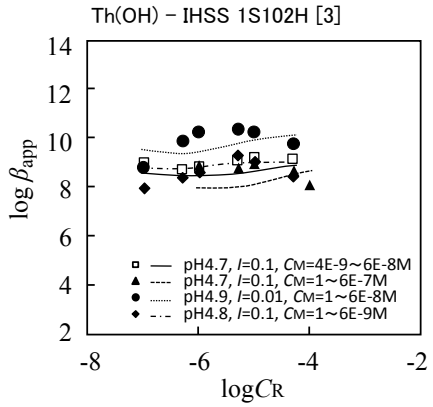

Fig.1. Example of comparison between the experimental apparent formation constants β_{app} of Th(IV) with humic acid (purchased from IHSS) and the simulated curves; C_R, molar concentration of HS, C_M, initial concentration of metal ion.

REFERENCES:
[1] Schulten, H. R., Schnitzer, M. Naturwissenschaften, **80** (1993) 29–30.
[2] Sasaki, T., Kobayashi, T., Takagi I., Moriyama, H. J. Nucl. Sci. Technol., **45** (2008) 718–724.
[3] Sasaki, T., Yoshida, H., Aoyama, S., Kobayashi, T., Takagi I., Moriyama, H. Radiochimica Acta. (2015) *in press*.

採択課題番号26P11-1　アクチニド元素の水溶液内錯生成反応に関する研究　　プロジェクト
（京大院・工）佐々木隆之、小林大志、鴻上貴之（京大・原子炉）上原章寛、藤井俊行、山名　元、森山裕丈

PR11-2 Temperature Effect on the Solubility and Solid Phase of Tetravalent Metal Hydroxide

T. Kobayashi, T. Sasaki, A. Uehara[1], T. Fujii[1], H. Yamana[1], H. Moriyama[1]

Graduate School of Engineering, Kyoto University
[1]Research Reactor Institute, Kyoto University

INTRODUCTION:

The decay heat emission from vitrified high level radioactive waste in the repository will be transferred to groundwater aquifers through surrounding engineered and geological barrier systems. In the early failure scenario of the waste package, long-lived radionuclides including tetravalent actinides (An(IV)) leached in the groundwater are considered to be exposed to an elevated temperature environment up to 100°C [1]. For the safety assessment of geological disposal, it is required to evaluate a possible impact of elevated temperature on the solubility of An(IV). At 25°C, the steady-state solubility is generally controlled by amorphous hydroxide as solubility-limiting solid phase, and described using relevant thermodynamic constants [1]. However, the amorphous hydroxide was dehydrated and crystalized at elevated temperature [2]. Therefore, the thermodynamic estimation of An(IV) solubility needs to clarify the both of hydrolysis constants and solubility product (K_{sp}) at a given elevated temperature [3].

In the present study, the apparent solubility of zirconium hydroxide as chemical analogue for An(IV) and the crystallinity of the solid phase were investigated under several conditions of temperature (5 to 60°C). The temperature dependence of solubility product and the enthalpy change were discussed.

EXPERIMENTS:

Sample solutions by oversaturation method were prepared by adding NaOH or $HClO_4$ to the acidic Zr perchlorate solutions ([Zr] = 0.01 mol/dm^3 (M)). The ionic strength (I) was adjusted to be I = 0.5 by adding appropriate amount of $NaClO_4$. After aging the sample solutions in temperature chambers controlled at 5°C, 40°C and 60°C, the samples were transferred to the thermostat dry-bath followed by the ultrafiltration and pH measurement at different temperature conditions. After filtration of supernatants through the ultrafiltration membranes (3 kDa – 100 kDa NMWL, Millipore), the apparent solubility of zirconium was determined by ICP-MS. XRD was used to characterize the crystallinity and the particle size of the solid phase.

RESULTS:

The apparent solubility after aging at 40 and 60°C and measured at 25°C were lower than those kept at 25°C, indicating the progress of crystallization of initial amorphous hydroxide. The K_{sp} values after aging at different temperatures were determined from the analysis of the solubility dataset in Fig.1. After aging at 60°C, the solubility was measured at 5, 25, 40 and 60°C (Fig. 2) and the K_{sp} at different temperatures. Assuming no temperature dependence of enthalpy change ($\Delta_r H^o$), the $\Delta_r H^o$ was calculated for $Zr^{4+} + 4OH^- <=> Zr(OH)_4$ (s,60°C), where $Zr(OH)_4$ (s,60°C) represents the solid phase formed at 60°C. The obtained $\Delta_r H^o$ was slightly higher than the $\Delta_r H^o$ (–133.6 kJ/mol) for $Zr(OH)_4$(am) calculated from the standard enthalpy of formation [3]. Similar analysis was performed for the solubility after aging at 5 and 40°C, and a trend of $\Delta_r H^o$ for the solid phases formed at different temperatures suggested that the solid phase transformation is endothermic reaction within the investigated temperature range.

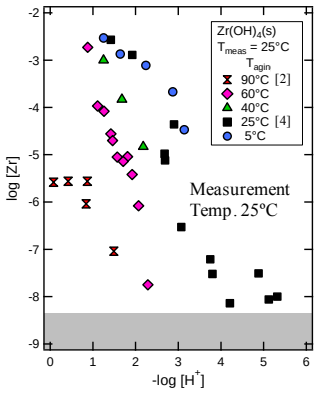

Fig. 1. Solubility of $Zr(OH)_4$(s) after aging at different temperatures.

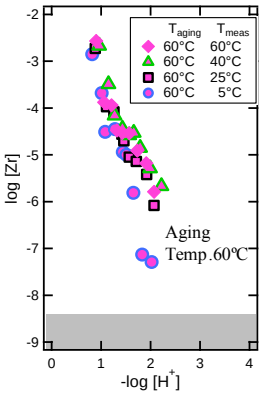

Fig. 2. Solubility of $Zr(OH)_4$(s) measured at different temperatures after aging at 60°C.

REFERENCES:

[1] 2nd progress report on research and development for the geological disposal of HLW in Japan, JNC Report TN1410 2000-001, JNC, Tokai, Japan.
[2] Kobayashi T. et al., Radiochim. Acta, 101, (2013) 645.
[3] Brown P. et al., Chemical Thermodynamics of Zirconium, Elsevier, North-Holland, Amsterdam (2005).
[4] Sasaki, T. et al., Radiochim. Acta 94, 489 (2006).

採択課題番号26P11-2 アクチニド元素および放射性核種の溶解沈殿反応に関する研究 プロジェクト
（京大院・工）小林大志、佐々木隆之（京大・原子炉）上原章寛、藤井俊行、山名 元、森山裕丈

PR11-3 Research on the Behavior of Actinides and FPs in Fuel Debris

N. Sato[1], A. Kirishima[1], M. Hirano, T. Sasaki[2], T. Kobayashi[2], Y. Takeno[2], A. Uehira[3], T. Fujii[3], K. Takamiya[3] and H. Yamana[3]

[1] *Institute of Multidisciplinary Research for Advanced Materials, Tohoku University*
[2] *Graduate School of Engineering, Kyoto University*
[3] *Research Reactor Institute, Kyoto University*

INTRODUCTION:

After the LOCA of Fukushima Daiichi NPS, the melted core reacted with coolant at high temperature forming fuel debris containing fuel and structural materials such as zirconium. Under high temperature condition in the pressure vessel, several kinds of FPs and TRU were possibly released into the cooling water mixed with seawater and the air from the melted core and its fine debris. Information on the radionuclide behavior in fuel debris and surface seawater will be helpful to analyze the forthcoming analysis data about the contents of minor FPs and TRU in contaminated water, and to manage associated secondary wastes. First, the simulated fuel debris composed of uranium and zirconium oxides as main constituents was prepared by heat treatment in reductive or oxidative conditions. Then the dissolution behavior of typical gamma-ray fission products and neutron activated nuclides as well as uranium in solid solutions was investigated by neutron irradiation and following leaching in the non-filtrated seawater. Dissolution behavior of MA was also studied by the used of MA doped simulated fuel debris.

EXPERIMENTAL:

Three types of UO_2-ZrO_2 solid solution samples with Zr concentration of 10, 50 and 90 mol% were prepared by mechanochemical and heat treatments under reductive and oxidative atmosphere. The sample was vacuum-sealed in quartz tube and irradiated for 20 min using the pneumatic transferring system (Pn-2) at KUR. For reducing the high radioactivity of short-lived nuclides, the sample was left in glove box, and then suspended in 30 ml of fresh seawater from Minamisoma city, Fukushima. After the aging time in the atmospheric condition at R.T., a 10 mL of supernatant was transferred to new sample tube after filtration with 0.45 μm (Advantec) or 3 kDa (Microcon, Millipore) membranes, followed by evaporation of the seawater at 363 K in order to repare a solidified point-like source. For MA doped sample, similar preparation techniques were applied by using U_3O_8 powder with ^{237}Np, ^{243}Am and ^{236}Pu. Gamma- and alpha- ray spectrometry were performed using a Ge detector and Si detector to determine the nuclides leached.

RESULTS:

Figure 1 shows the leaching ratios (R(%)) of actinides to seawater. There, the clear time dependence cannot be seen in the leaching of Np, Am and Pu during 31 days leaching test. Also, their leaching ratios were supressed in the very low extent (0.02 % or less). The leaching of these actinides are expected to be supressed to very low extent regardless of the oxidation state in the solid phase since the solubilities of both M(III) and M(IV) for Am and Pu, and Np~~(IV)~~ are very low at the pH of seawater. On the other hand, the R_U value was about 0.1 % during the leaching test. From this result, it is considered that the uranium dissolution from the simulated fuel debris was governed by the solubility limitation of UO_3 $2H_2O$(cr), UO_3・$2H_2O$ (am) or maybe their intermediate phase as discussed in our previous study [1]. These results suggest that both dissolution and structure data are essential for fuel debris behaviour. In further study, behavior of actinides and FP's from different types of fuel debris will be discussed.

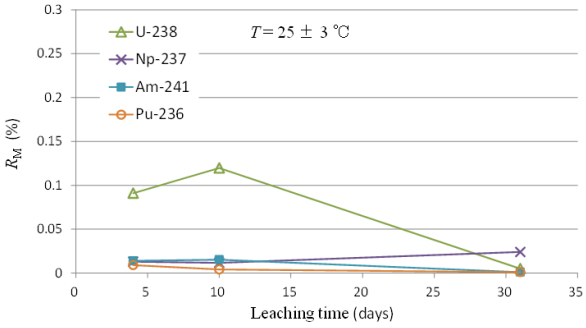

Figure 1 Time dependence of actinides leaching from the simulated fuel debris to the Fukushima seawater [2].

REFERENCES:

[1] T. Sasaki, Y. Takeno, A. Kirishima, N. Sato, J. Nucl. Sci. Technol., 52 (2015) 146-150.
[2] A. Kirishima, M. Hirano, T. Sasaki, N. Sato, J. Nucl. Sci. Technol., in press, doi: 10.1080/00223131.2015.1017545.

採択課題番号 26P11-3　　燃料デブリ中のアクチノイドおよび FP 元素の挙動に関する研究プロジェクト　（東北大多元研）佐藤修彰、桐島　陽、平野正彦（京大院工）佐々木隆之、小林大志、竹野　佑（京大・原子炉）上原章寛、藤井俊行、高宮幸一、山名　元

PR11-4 Effect on Borosilicate Glass Structure by Neutron Irradiation

T. Nagai, A. Miyauchi, Y. Morikawa, A. Uehara[1], and T. Fujii[1]

Japan Atomic Energy Agency (JAEA)
[1]Research Reactor Institute, Kyoto University

INTRODUCTION: A high-level radioactive liquid waste including fission products, FPs, from a reprocessing process for spent nuclear fuels is processed into a solidified waste glass made by using a borosilicate glass as media. Many studies of the effect on borosilicate glass structure by irradiation have been carried out by irradiation of α ray, β ray, and γ ray which would be generated from FPs of the waste glass. However, that effect by a neutron irradiation has not been much evaluated. In this study, the borosilicate glass samples were irradiated by neutrons, and the glass structure change after the irradiation was measured by Raman spectrometry.

EXPERIMENTS: The borosilicate glass samples were prepared 2 compositions. The raw material reagents of SiO_2, H_3BO_3, Na_2CO_3, Li_2CO_3, and rare earth oxides as simulated FPs were placed in an alumina crucible and were melted at 1150°C in an electric furnace. After the molten samples were solidified by cooling to room temperature, they were cut into thin plates. In the irradiation, the glass samples of thin plate were set in a polyethylene tube and were irradiated under the condition of 1000 kW for 10 min in the Pn-2 of KUR. After the radioactivity of the samples was sufficiently attenuated, the Raman spectra of the glass sample were measured by using a laser Raman spectrometer, NRS-3100 of JASCO. For the effect on borosilicate glass by the nuclear reaction of $^{10}B(n,\alpha)^7Li$, Peuget, *et al* have evaluated the B-O structure by using NMR measurement and Raman spectrometry[1], our study was examined the Si-O structure.

RESULTS: As a structural change of the sample by the irradiation, an amount of Li would be increased by the $^{10}B(n,\alpha)^7Li$ reaction, and Li was expected to disconnect to the Si-O bridging structure. By evaluating the Raman shift of the Si-O structure, it was confirmed to be the effect on the borosilicate glass structure by the irradiation. The Raman shifts of Si-O structure of a silicate glass were in the wavenumber of 850-1200 cm^{-1}, and the peak positions of Raman shifts were different from the number of non-bridging oxygen, NBO, of the Si-O structure.[2] In this measurement of borosilicate glass, those Raman shifts were observed in 850-1250 cm^{-1} and the measured spectra could be separated into Gaussian waves as shown in Fig. 1. The Raman peak of Q^4 structure without NBO appeared in 1140-1150 cm^{-1}, and those of Q^3, Q^2, and Q^1 structures with the NBO number = 1, 2, and 3 were in 1070-1090, 1000-1020, and 920-930 cm^{-1} respectively. Comparing with the Raman shifts before and after irradiation, it could be observed that the peak heights of Q^4 and Q^3 decreased and those of Q^2 and Q^1 increased after the irradiation, as shown in Fig. 1. These height changes of Q^n, n=1-4, suggested the feasibility that a generated Li by the neutron irradiation disconnects the Si-O bridging structure in a borosilicate glass. However, this Si-O bridging structure is direct disconnected by γ ray included in the neutron irradiation and the additional experiments needs for understanding of the irradiation effect.

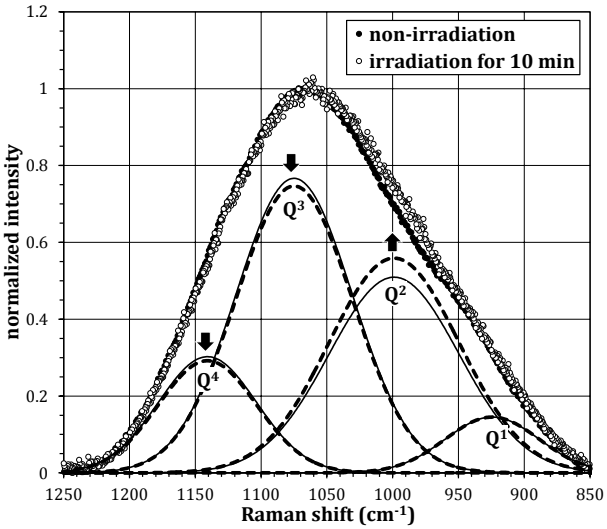

(1) $63SiO_2$-$16.6B_2O_3$-$19Na_2O$-$1.4RE_2O_3$.

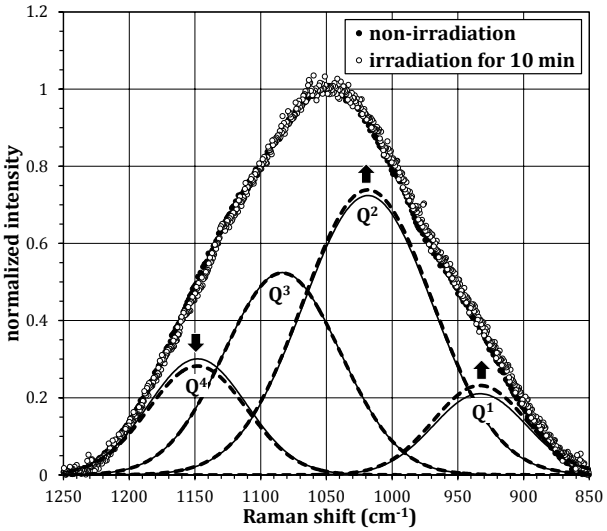

(2) $63SiO_2$-$16.6B_2O_3$-$8.1Li_2O$-$10.9Na_2O$-$1.4RE_2O_3$.

Fig. 1. Raman spectra of glass samples and their separated Gaussian waves. Open circles and fine lines are a non-irradiation sample, and closed circles and dotted lines are after irradiation.

REFERENCES:

[1] S. Peuget, et al, Nucl. Inst. Methods in Phys. Res. B, **327** (2014) 22-28.
[2] P. McMillan, Am. Mineralogist, **69** (1984) 622-644.

採択課題番号 26P11-4 中性子照射によるホウケイ酸ガラス構造への影響評価 プロジェクト
（原子力機構）永井崇之、守川 洋、宮内厚志（京大・原子炉）藤井俊行、上原章寛

PR11-5 Ligand Exchange of Uranium (IV) Chloro- and Fluoro- Complexes in High Temperature Molten NaCl-CsCl Eutectic

A. Uehara[1], T. Nagai[2], T. Fujii[1], H. Moriyama[1], and H. Yamana[1]

[1] Research Reactor Institute, Kyoto University
[2] Nuclear Fuel Cycle Engineering Lab., Japan Atomic Energy Agency

INTRODUCTION:

In the non-aqueous reprocessing process of spent nuclear fuels by the pyrometallurgical and the electrowinning methods, a spent fuel is dissolved into molten LiCl-KCl or NaCl-CsCl eutectic melt and dissolved uranium and plutonium ions are recovered as metal or oxide. In the present study, the chemical property and coordination circumstance of the complexes of U^{4+} under the coexistence of fluoride ions in molten NaCl-CsCl eutectic were investigated by absorption spectrum measurements.

EXPERIMENTAL:

All experiments were carried out under an argon atmosphere, in which humidity and oxygen impurity were continuously kept less than 1 ppm. The electronic absorption spectra of uranium ions in the melts were measured by using an UV/Vis/NIR spectrometer (V-570, JASCO Co.). The analytical light from a light source (a tungsten halogen lamp and D_2O lamp) was guided to the electric furnace with quartz windows by using optical fibers, and the light passed through the sample in a quartz tube with a 10 mm light path inside the furnace. The light which traveled through the furnace was again guided to the spectrophotometer, and a monochromator was set in front of the detectors to decrease the background noise. The light intensity for the molten alkali chloride (I_0) and that including uranium (I) was measured in the wavelength range of 300 – 2000 nm at 1 nm intervals. Wavelength was converted to wavenumber in this work. The molar absorptivity was calculated by using $-\log(I/I_0)$ and total volume of the solution. All the experiments were performed at 923K ± 3K.

RESULTS:

Molar absorptivity of absorption spectra of U^{4+} in the presence of F^- was plotted as a function of wavenumber in Fig. 1. When an absorption spectrum of 0.106 M U^{4+} in the absence of F^- was measured, molar absorptivities of each peak wavenumber at 14903, 16501 and 22123 cm^{-1} agreed with the reported values [1]. By comparing these values with the crystal field analysis data of U^{4+} in $CsCdBr_3$ [2] and $LiYF_4$ [3], absorption bands of the $5f^2$-$5f^2$ transition of U^{4+} were assigned as follows; the $^1I_6 \leftarrow {}^3H_4$ transition at 22500-19000 cm^{-1}, the $^3P_1 \leftarrow {}^3H_4$ transition at 17800 cm^{-1}, the $^1G_4$, $^1D_2$, $^3P_0 \leftarrow {}^3H_4$ transition at 17000-14000 cm^{-1}, the $^3H_6 \leftarrow {}^3H_4$ transition at 13100-12000 cm^{-1}, the $^3F_3$, $^3F_4 \leftarrow {}^3H_4$ transition at 11100-7500 cm^{-1}, and the $^3H_5 \leftarrow {}^3H_4$ transition at 6500-5000 cm^{-1}.

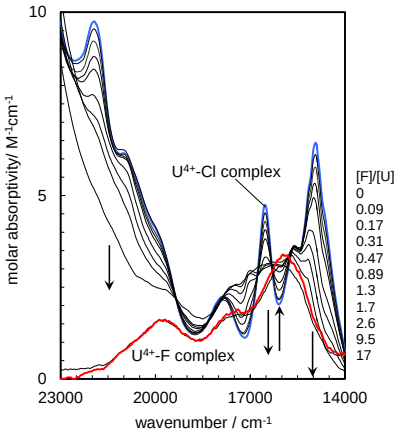

Fig. 1. Molar absorptivity of U^{4+} depended on the concentration of NaF in molten NaCl-CsCl eutectic at 923K. Concentration ratios of F^- by U^{4+} (r_F) are 0, 0.09, 0.17, 0.31, 0.47, 0.89, 1.3, 1.7, 2.6, 9.5, and 17.

When 9.36×10^{-3} M NaF was added in the melt, absorption peaks decreased. Molar ratio of fluorine by uranium (r_F) added in the melt was changed from 0.09 to 17 by adding NaF pellet as shown in Fig. 1. Absorption peaks corresponding to 14903, 16501, and 22123 cm^{-1} decreased with the increase of r_F from 0.09 to 1.7 and isosbestic points at 13774, 15772, 16181, 17793, and 19305 cm^{-1} were observed. This result means that two species of complexes composed of U^{4+}, Cl^- and F^- are equilibrated. However, when r_F was over 9.5, another peaks at 15847, 17331, and 19646 cm^{-1} were observed. This indicates that another complex composed of U^{4+}, Cl^-, and F^- is formed. After 10 hours aging, red color precipitates were found on the bottom of the cell.

REFERENCES:

[1] Nagai, et al., *J. Nucl. Sci. Technol.*, **42**, 1025-1031 (2005).
[2] Karbowiak, et al., *Chem. Phys.*, **308**, 135-145 (2005)
[3] Hubert, et al, *J. Luminescence*, **60&61**, 245-249 (1994)

採択課題番号 26P11-5　　イオン液体中におけるアクチニドイオンの溶存状態研究　　プロジェクト
（京大・原子炉）上原章寛、藤井俊行、森山裕丈、山名 元（原子力機構）永井崇之

PR11-6

Evaluation of Parameters Governing Anodic Dissolution of U-Zr Alloy in Molten LiCl-KCl

M. Iizuka[1], Y. Sakamura[1],
T. Fujii[2], A. Uehara[2] and H. Yamana[2]

[1]*Central Research Institute of Electric Power Industry*
[2]*Research Reactor Institute, Kyoto University*

INTRODUCTION: Analyses of the electrorefining process for the pyrometallurgical reprocessing of metallic fast reactor fuel using the multi diffusion layer anode model [1] have shown that (a) solubility of UCl_3 in LiCl-KCl melt, and (b) the diffusion coefficient of actinide ions in the porous Zr layer formed at the surface of the spent metallic fuel by selective dissolution of the actinides, have great influence on major performance, such as processing rate and separation between the actinides and Zr. In this study, chronopotentiometry (CP) was applied to evaluation of these important parameters at U-9wt%Zr alloy anode.

EXPERIMENTS: Modification of CP theory to be adapted to a situation, where the concentration reaches saturation by a constant current producing the species electrochemically, has been reported before [2]. Since diffusion coefficient of U(III) in LiCl-KCl is known [3], solubility of UCl_3 in LiCl-KCl was evaluated using this data and τ obtained by CP in this study. After formation of a porous Zr layer by selective anodic dissolution of U from the U-Zr alloy, CP was performed again. In this step, theoretically, the effective diffusion coefficient of UCl_3 in the porous Zr layer can be estimated using its solubility data which has been just evaluated in the previous step. The experimental setup and procedure have been also reported before [4]. All the experiments were carried out at 773 K, in a high-purity Ar atmosphere glove box in KURR hot cell laboratory.

RESULTS: The CPs obtained using U-Zr alloy before the formation of the porous Zr layer are shown in Fig. 1. The solubility of UCl_3 was evaluated to be 0.00449 mol-U/cm^3 so that its averaged diffusion coefficient determined from these CPs agrees with the value in literature (1.45×10^{-5} cm^2/s) [3]. Subsequently, CPs were measured after the formation of the porous Zr layer. In this case, the diffusion coefficient could not be evaluated directly from τ value, since the period until diffusion limit of U(III) varied in every measurement even with the same current density, as shown in Fig. 2. The reason for this behavior was considered that the decay of UCl_3 concentration gradient in the porous Zr layer caused by the CP measurement requires a long duration due to the expected lower diffusion coefficient and the large thickness of the layer. Such complicated condition and resulting behavior in the actual CP measurement cannot be explained using either the basic electrochemical theory [2] or simple multi-diffusion layer model [1]. Then, the series of the electrochemical operations, including the CP measurement at constant current density and the rest period in open circuit situation between the measurements, were digitally simulated by discretization of the diffusion layers around the U-Zr alloy into elements of 10 to 20 μm thickness using finite element method. The calculation result indicated that the transition time evaluated from CPs shown in Fig. 2 can be properly reproduced by assuming the effective diffusion coefficient of U(III) in the porous Zr layer to be $0.6 \sim 0.8 \times 10^{-5}$ cm^2/s, which is consistent with the value 0.7×10^{-5} cm^2/s evaluated from the analysis of the longer-term electrorefining experiments [1].

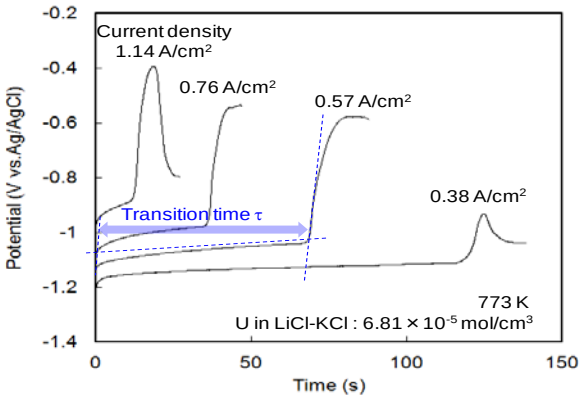

Fig. 1. Chronopotentiograms obtained with U-Zr alloy before formation of porous Zr layer.

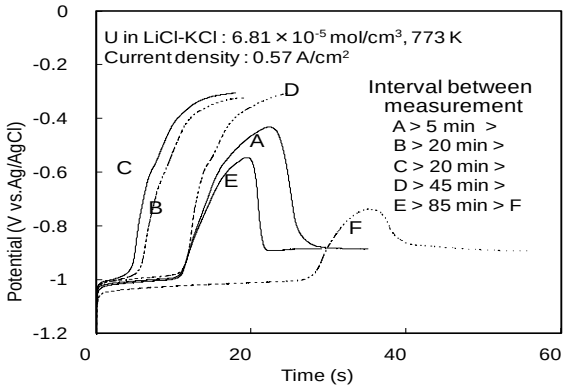

Fig. 2. Chronopotentiograms obtained with U-Zr alloy after formation of porous Zr layer.

REFERENCES:

[1] M. Iizuka *et al.*, J. Nucl.Sci.Technol., **47** (2010) 1140.
[2] M. Iizuka *et al.*, KURR annual report 2010.
[3] S. A. Kuznetsov, *et al.*, Electrochim. Acta, **51** (2006) 2463.
[4] M. Iizuka *et al.*, KURR annual report 2005.

採択課題番号 26P11-6 乾式再処理に関するウラン化合物を用いた基礎研究　　プロジェクト
（電中研）坂村善治、飯塚政利、魚住浩一、村上　毅
（京大・原子炉）藤井俊行、上原章寛、山名　元

PR11-7 Electrochemistry and Structural Analysis of Cations in Molten Subhalide Systems: Fluoride Addition Effect on Voltammograms and UV-vis Spectra of Neodymium Cation in Molten Chlorides

H. Matsuura, A. Nezu, H. Akatsuka, A. Uehara[1], H. Yamana[1], T. Fujii[1]

Research Laboratory for Nuclear Reactors, Tokyo Institute of Technology
[1]Research Reactor Institute, Kyoto University

INTRODUCTION: Neodymium is the one of the rare earth fission products and was used as the prototype of some trans uranium elements due to its similarity of electrochemical behavior. Also, neodymium is one of important materials since it has been widely utilized at magnets in the motors, and effective recycling technology from the end products has been waiting for a long time. Although molten salt should be relatively constructed by a simple structural model due to the predominant ionic species in liquid phase, electrochemical behavior has not been well understood by the microscopic point of view. For a recent few years, the electrochemical behavior of rare earths including neodymium in the molten chlorides with small amount of fluorides has been focused, and structural elucidation by extended absorption fine structure and UV-vis spectroscopy of neodymium in molten salts has been performed [1,2]. In this year, fluoride concentration dependence on the voltammograms of neodymium in molten LiCl-KCl and spectra of neodymium in molten NaCl-2CsCl was remeasured and the structural variation is discussed newly by some parameters derived from the Judd-Ofelt analysis.

EXPERIMENTS: All the electrochemical experiments using molten salts have been performed in an electric furnace which is built inside a glove box filled with an argon atmosphere in high purity using an electrochemical analyzer. Cyclic voltammetry, differential pulsed voltammetry and linear sweep voltammetry have been performed by using the electrodes as follows: working electrode: tungsten, counter electrode: pyrocarbon and reference electrode: silver wire dipped in molten LiCl-KCl eutectic + AgCl (1 mol%) inside the borosilicate tube, respectively. Silica glass tube was used as a crucible. To observe the fluoride addition effect, 0 to 20 times amount of LiF to the concentration of neodymium was added to the molten salt. All measurements have been performed at 773 K. UV-vis spectroscopy of neodymium in molten NaCl-CsCl-NaF at 953 K has been carried out by using the spectrophotometer. A quartz cell with 10 mm of light path was used for the molten salt container, and experimental procedure was exactly the same as that described in the report of the last year. For the calculation of oscillator strength of the hypersensitive transition and derivation of $\Omega_{2,4,6}$ parameters by the Judd-Ofelt analysis, density was assumed to be the additivity of molar volume of each component, and refractive index was temporary used from the value of KCl due to the non-availability of the data of CsCl.

RESULTS and DISCUSSION: Figure 1 shows the differential pulsed voltammograms of cathodic sweeps which exhibit mainly neodymium reduction peaks. On the contrary to previous measurements[1,2], the potential of neodymium reduction to metal was not shifted positively, however, drastic negative shift depending on fluoride addition did not occur as well. More strikingly, with increasing fluoride amount, the potenital gap between Nd^{3+}/Nd^{2+} and Nd^{2+}/Nd decreased, thus disproportionation reaction may be restricted by addition of fluoride. The variation of oscillator strength of hypersensitive transition absorption of neodymium at ca. 589 nm depending on fluoride addition has been evaluated. This absorption peak has been considered to the indication of coordination symmetry around neodymium cation, i.e. 6 coordinated octahedral species, and the smaller value relates to more perfectly symmetric. One striking feature is that with increasing fluoride amount until ca. F/Nd = 2 in molten NaCl-CsCl-NaF, the value of oscillator strength once increases until F/Nd = 2, and decreases rapidly. While in molten LiCl-KCl-LiF, the value of oscillator strength decreases almost linearly.

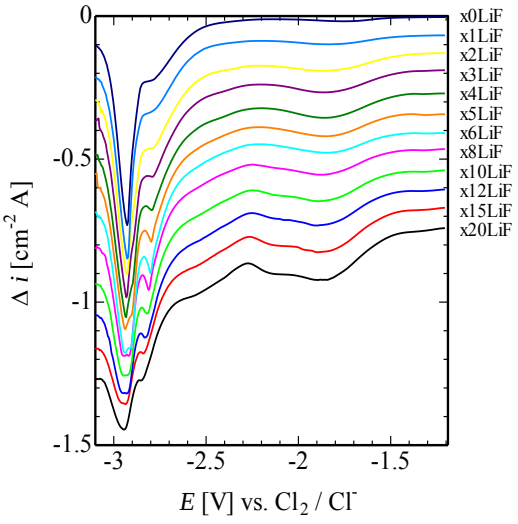

Fig. 1 Differential pulsed voltammograms of cathodic sweeps of neodymium in molten LiCl-KCl-LiF.

REFERENCES:

[1] Y. Shimohara *et al*, Molten salt chemistry and technology, John Wiley & Sons (2014) 577.
[2] K. Fujita *et al*, Proc. AMS4, (2012) 264.

採択課題番号 26P11-7　アクチニド元素及びFP元素含有ハロゲン化物のXAFS構造解析 プロジェクトおよび可視紫外分光研究

（東工大・原子炉研）松浦治明、根津　篤、赤塚　洋　（京大・原子炉）上原章寛、山名 元、藤井俊行

PR11-8 Polarization Effect of Chloride Ions on Uranyl Ion in Molten LiCl

N. Ohtori, Y. Ishii, A. Uehara[1], T. Fujii[1], H. Yamana[1]

Department of Chemistry, Niigata University
[1]Research Reactor Institute, Kyoto University

INTRODUCTION: Molten salts are promising solvents for actinides in reprocessing of nuclear fuel. However, knowledge of chemical stability of ionic species in melts is still inadequate to maximize their potential abilities. Information on local structure around ionic species in melts may provide useful measures for their stability in melts. Molecular dynamics (MD) simulation is a powerful tool to elucidate such structures microscopically. In particular, recent MD simulations with polarizable ionic model (PIM)[1,2] have brought much progress in understanding of structure in ionic melts: they have successfully revealed more reliable picture of local structure in UCl_3[2] which is comparable with those from XRD study. In this work, we have performed MD calculations of molten LiCl containing uranyl ion using PIM for chloride ions, and investigated the effect of polarization of Cl^- ions on local structures around uranyl ion.

CALCULATION: MD calculations have been carried out using PIM for molten LiCl containing UO_2^{2+} ion. The system included 500, 502, and 1 ions for Li^+, Cl^-, and UO_2^{2+}, respectively. MD calculation without polarization of Cl^- ions has also performed, which is referred here to as RIM: rigid ion model. Furthermore, first principle MD simulation has been performed using the CPMD code[3] for the system with similar composition but smaller size. The temperature was set at 1073 K in all the calculations.

RESULTS: Figures 1 and 2 show radial distribution functions for U and Cl pair and U and Li pair, respectively, obtained from the present calculations. Table 1 summarizes intraionic distance between U and O in uranyl ion and interionic distance between U and Cl which are near neighbors with each other. These results clearly show effects of polarization of Cl^- ions on the coordination structures around uranyl ion. That is, we have found that PIM can reproduce the results by first-principle MD simulation better than RIM.

Table 1 Intraionic distance between U and O in uranyl ion and interionic distance between U and Cl in molten LiCl containing uranyl ion

	Expt.	CPMD	PIM	RIM
U=O	1.77 Å	1.80 Å	1.78 Å	1.77 Å
U-Cl	2.73 Å	2.64-2.71 Å	2.78 Å	2.94 Å

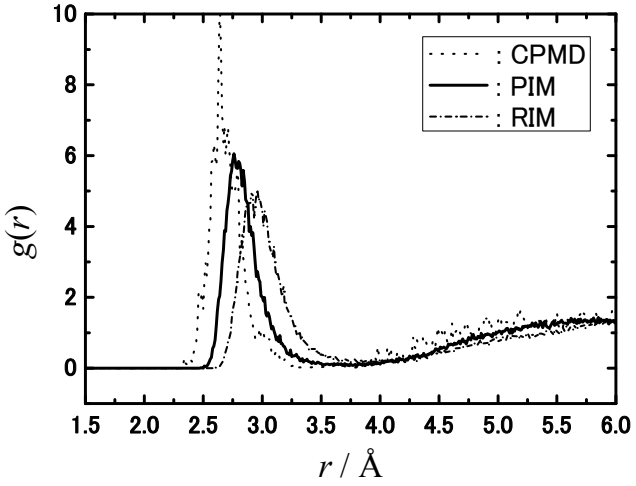

Fig.1 Radial distribution functions for U and Cl pair obtained from the present calculations.

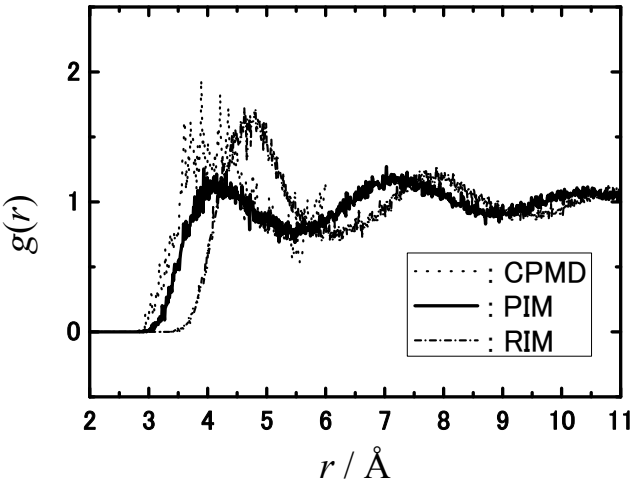

Fig.2 Radial distribution functions for U and Li pair obtained from the present calculations.

REFERENCES:

[1] P. A. Madden, R. Heaton, A. Aguado and S. Jahn, J. Mol. Struct.:THEOCHEM, **771** (2006) 9-18.
[2] Y. Okamoto, P. A. Madden and K. Minato, J. Nucl. Mater. 344 (2005) 109-114.
[3] http://www.cpmd.org/

採択課題番号 26P11-8　融体中での f-元素の分子動力学計算と実験系の照合研究　プロジェクト
（新潟大・理）大鳥範和、石井良樹　（京大・原子炉）上原章寛、藤井俊行、山名　元

PR11-9

Study of Isotope Separation of Strontium and Calcium via Chemical Exchange Reaction

R. Hazama, Y. Sakuma[1], A. Ito, T. Fujii[2], S. Fukutani[2], Y. Shibahara[2]

Graduate School of Human Environment, Osaka Sangyo University
[1]Research Laboratory for Nuclear Reactors, Tokyo Institute of Technology,
[2]Research Reactor Institute, Kyoto University

INTRODUCTION: Anomalous mass dependence was experimentally observed in uranium isotope fractionation by Fujii et al., in the late 80's[1] and Nishizawa et al., suggested that odd-even staggering may be due to the nuclear charge density difference in the middle of 90's[2] for the case of strontium. Calcium is congener of strontium and easy to handle to check the isotope effects[3,4].

EXPERIMENTS: Isotopic enrichment occurs according to the following chemical exchange reaction:
$^{40}Ca^{2+}_{(aq)} + {}^{48}CaL^{2+}_{(org)} \rightarrow {}^{48}Ca^{2+}_{(aq)} + {}^{40}CaL^{2+}_{(org)}$ (1)
where L represents macrocyclic polyether(18-crown-6). As a result, ^{40}Ca is enriched in the organic-phase (org) crown solution and the heavy isotopes of ^{48}Ca tend to concentrate in the aqueous (aq) phase. The mass effect is observed by the thermal ionization mass spectrometer (TIMS) measurement of calcium isotope ratios for the mass range from 40-48 atomic mass unit (amu).

RESULTS: Unit mass enrichment factors of Sr and Ca isotope separation are summarized in Table 1. In general, a crown ether gives a large separation factor with more than ten times, compared with an ion exchange method and has an applicable ability of separation in reality.

ε /△M [$\times 10^{-5}$]	Method and system	Temp. (℃)	Ref.
51-17 (Sr)	Liquid-liquid extraction (LLE) with dicyclohexano-18-crown-6 (DC18C6). 2.3M-0.5M Sr in aqueous phase.	20±0.5	[2]
14 (Sr)	Crown-ether resin chromatography (CRC). 1.3m 0.1-0.01M Sr + 2M HCl	35±2	[5]
5.6 (Sr)	CRC. 1.3m 0.1M Sr + 3M HNO_3	35±2	
2.3 (Sr)	α -hydroxyisobutyrate	Not specified	[6]
0.31 (Sr)	Cation-exchange chromatography with Sr lactate.	25±0.2	[7]
100 (Ca)	LLE with DC18C6. 0.07M $CHCl_3$	25	[8]
36-15 (Ca)	LLE with HDEHP(di(2-ethylhexyl) orthophospheric acid)	10-50	[9]
130 (Ca)	LLE with amalgam. 0.27-0.68M Ca/liter Hg	25	[10]
2.3 (Ca)	Ion exchange chromatography with Dowex50	room temp.	[11]
98 (Ca)	CRC(cryptand2B.2.2). 0.01M $CaCl_2$+CH_3OH/$CHCl_3$	20	[12]
63 (Ca)	CRC (18C6) 0.01M $CaCl_2$+CH_3OH/$CHCl_3$	20	
2.8 (Ca)	Iminodiacetate resin 0.95M NaCl+0.05M $CaCl_2$	25	
56-130 (Ca)	CRC (cryptand2B.2.2) CH_3OH/$CHCl_3$/H_2O	-21-21	[13]
24 (Ca)	CRC (benzo-18C6). 0.02M Ca + 9M HCl	30	[14]
76 (Ca)	CRC (benzo-18C6). 9M HCl (0.8mm φ ,1m)	40	[15]
8.9 (Ca)	CRC (benzo-15C5). 12M HCl (0.8mm φ ,1m)	50	
150 * (Ca)	LLE with DC18C6 0.07M $CHCl_3$	20	This work

Table 1. Unit mass enrichment factors of Sr and Ca isotope separation. *: Preliminary

REFERENCES:

[1]Y. Fujii *et al*., Z. Naturforsch., **44a** (1989) 395.
[2] K. Nishizawa *et al.*, J. Nucl. Sci. Technol., **32** (1995) 1230.
[3] R. Hazama *et al*., Proc. of 6th Rencontres du Vietnam, Gioi Publishers (2007) 383: arXiv0710.3840.[nucl-ex].
[4] Y. Fujii *et al.*, Isotopes in Environmental and Health Studies, Vol. **46**, No.2, (2010) 233.
[5] Y. Ban *et al*., Sep. Sci. Technol. **36**(2001)2165.
[6] J. Aaltonen, Suom. Kem., **B45** (1972) 141.
[7] T. Oi *et al*., Sep. Sci. Technol., **27** (1992) 631.
[8]B.E. Jepson *et al*., J. Inorg. Nucl. Chem.**38**(1976)1175.
[9]E.P. Horwitz *et al*., J. Chromatography **125**(1976)203.
[10]D. Zucker *et al.*, J. Chem. Phys. **41**(1964)1678.
[11] B.E. Jepson *et al*., Sep. Sci. Technol. **19**(1984)173.
[12] B.E. Jepson *et al*., Sep. Sci. Technol. **25**(1990)1893.
[13]K.G. Heumann *et al*., Angew. Chem. Int. Ed. Engl. **19**(1980)406.
[14]K. Hayasaka *et al*., Prog. Nucl. Energ. **50**(2008)510.
[15]S. Nemoto *et al*., J. Nucl. Sci. Tech. Vol. **49**, No. 4, (2012) 425.

採択課題番号26P11−10 ストロンチウム及びカルシウムの化学交換法における同位体分別研究 プロジェクト

（大産大院・人間環境）硲　隆太、伊藤彩　（東工大・原子炉研）佐久間洋一
（京大・原子炉）藤井俊行、福谷哲、芝原雄司

PR11-10 Experimental and Calculated Optical Properties of Molten Alumnium Chloride Melts

T. Goto, K. Hachiya[1], A. Uehara[2], T. Fujii[2], H. Yamana[2]

Graduate School of Science and Engineering, Doshisha University
[1]Graduate School of Energy Science, Kyoto University
[2] Research Reactor Institute, Kyoto University

INTRODUCTION: Molten $AlCl_3$ and *A*Cl-$AlCl_3$ (*A*: alkaline metals) have been attractive targets of studies from both fundamental and application viewpoints, because of their relatively low melting points which lead to their effectiveness. The structure of the melts contains a variety of coordinations which have long been investigated and mainly consists of covalent bonding between Al-Cl. In this study, Raman scattering measurements are performed to investigate into their bonding structures, and the spectra are analyzed with *ab initio* simulations. We focus our study on CsCl-$AlCl_3$ binary and LiCl-KCl-CsCl-$AlCl_3$ ternary systems

EXPERIMENTS: Raman scattering spectra obtained in KURRI were simulated by calculations with GAUSSIAN09 simulation package. Up to 2 ps trajectories of ions in the melts were calculated with a variant of first-principle molecular dynamics simulations, ADMP (Atom-centered Density Matrix Propagation). The computations of the ionic trajectories were performed for CsCl-$AlCl_3$ at 700 K.

RESULTS: As comprehensively reviewed in Ref. [1], up to 1 : 1 mixture of CsCl/$AlCl_3$ is expected to exclusively contain $AlCl_4^-$ cluster as an anion. On the other hand, $Al_2Cl_7^-$ clusters were contained 9.6% of the total anions in the whole snapshots, while $AlCl_4^-$ clusters were 73.4%. These numbers of anion rates show that $AlCl_4^-$ clusters are not always rigid, and Cl^- ions are exchanged among clusters.

Using Einstein relation for the mean square displacements versus time presented in FIG.1, self-diffusion constants were computed to be D_{Cs} = 1.216 x 10^{-4} cm^2 s^{-1}, D_{Al} = 1.530 x 10^{-4} cm^2 s^{-1} and D_{Cl} = 2.671 x 10^{-4} cm^2 s^{-1}, respectively. As far as we know, there is no direct reference experimental data for this system, while interdiffusion constant for NaCl-$AlCl_3$ mixture were reported to be 4.5 x 10^{-6} cm^2 s^{-1} at 413 K [2]. The square displacements for each individual atom are presented in FIG. 2. Al atoms, center of each anion clusters, exhibit both diffusing and static dynamics. A part of Cl atoms corresponds to Al atoms, both for two diffusing Al's and remaining non-diffusing two. Nevertheless, the rest of Cl's cannot be categorized to either of them. This result also supports that Cl^- ions are exchanged among clusters.

DISCUSSIONS: For CsCl-$AlCl_3$ mixture system, anion structure of isolate $AlCl_4^-$ tetrahedra shift to corner-sharing two-tetrahedron structure, $Al_2Cl_7^-$, dramatically at 1 : 1-ratio with increasing CsCl content. Our calculation seems to reproduce fluctuations in the structural rearrangement at that mixing ratio.

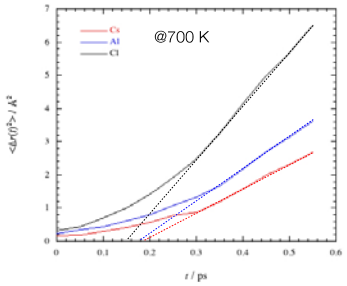

FIG. 1 Mean square displacements versus time for ADMP dynamics of constituent atoms at 700 K.

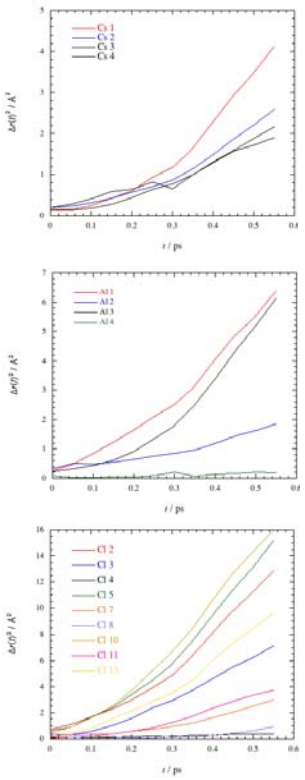

FIG. 2 Square displacements versus time for ADMP dynamics of Cs, Al and Cl atoms at 700 K.

REFERENCE:

[1] M. P. Tosi, D. L. Price, M.-L. Saboungi, *Annu. Rev. Phys. Chem*. **44** 173 (1993).
[2] B. Gilbert, D. L. Brotherton and G. Mamantov *J. Electrochem. Soc.* **121** 773 (1974).

採択課題番号26P11-11　　f 一元素の有効利用に関わる基礎及び応用研究　　プロジェクト
（同志社大・理工）後藤琢也（京大院・エネ科）蜂谷　寛（京大・原子炉）上原章寛、藤井俊行、山名　元

PR11-11 Precipitation Behavior of Trivalent Dysprosium Ion by Reaction with Oxide Ion in $CaCl_2$–LiCl Molten Salt

H. Sekimoto, A. Uehara[1], T. Fujii[1], H. Yamana[2]

[1]Faculty of Engineering, Iwate University Department of Materials Science and Engineering
[2]Graduate School of Science, Kyoto University[4]Research Reactor Institute, Kyoto University

INTRODUCTION: Development of recycling technique for neodymium magnet is essentially important to achieve sustainable society. Consequently, we propose and are investigating a new recycling process of neodymium magnet using B_2O_3 flux [1]. In the process, the neodymium magnet is melted together with sufficient amount of B_2O_3 in graphite crucible to form molten iron based alloy, B_2O_3 slag and Nd_2O_3-B_2O_3 slag, which is recovered and dissolved in molten salt. And then, Fe-Nd-B alloy is produced by electrolysis. For the process, thermodynamic properties such as solubility of rare earth oxide in molten salt is important information. In this study, precipitation behavior of dysprosium with adding oxide ion in $CaCl_2$-LiCl eutectic molten salt was investigated by spectrophotometry.

EXPERIMENTS: Solidified samples of $CaCl_2$-LiCl eutectic molten salt and 5 mol%Li_2O-$(CaCl_2$-LiCl$)_{eu.}$ molten salt were prepared through the following procedure. Li_2O, $CaCl_2$ and LiCl was weighted, mixed, co-melted at 700 °C in cylindrical quartz tube and quenched in Ar atmosphere. 3.01 g of $CaCl_2$-LiCl eutectic molten salt was inserted in a quartz optical cell and melted at 700 °C. The intensity of the transmitted light through $CaCl_2$-LiCl eutectic molten salt using a tungsten lamp and a spectrophotometer. Then, adding small amount of $DyCl_3$ in the $CaCl_2$-LiCl molten salt and measuring the intensity of the transmitted light through $DyCl_3$-$(CaCl_2$-LiCl$)_{eu.}$ molten salt was carried out repeatedly to obtain absorption spectra of Dy^{3+} at 700 °C. After that, adding small amount of adding Li_2O-$CaCl_2$-LiCl molten salt and measuring the intensity of the transmitted light through Li_2O-$DyCl_3$-$CaCl_2$-LiCl molten salt was also carried out repeatedly to obtain absorption spectra of Dy^{3+} at 700 °C. Using the data on the intensity of the transmitted light, absorbance was evaluated.

RESULTS: Figure 1 shows the absorption spectra of Dy^{3+} in $DyCl_3$-$(CaCl_2$-LiCl$)_{eu.}$ molten salt at 700 °C. There are three absorption peak depending on the concentration of Dy^{3+} in the range of wavelength, λ, from 800 nm and 1600 nm; a strong absorption peak at 1296 nm and 2 weak absorption peaks at 918 and at 1121. Figure 2 shows the absorption spectra of Dy^{3+} in Li_2O-$DyCl_3$-$CaCl_2$-LiCl molten salt. The spectra were shifted upward and the difference between the top of the absorption peak and the absorbance on the tangential line between the feet of the peak at around 1296 nm became smaller with introducing O^{2-}. These indicates that the formation of DyOCl or Dy_2O_3(s) proceeded and the amount of Dy^{3+} in molten salt decreased.

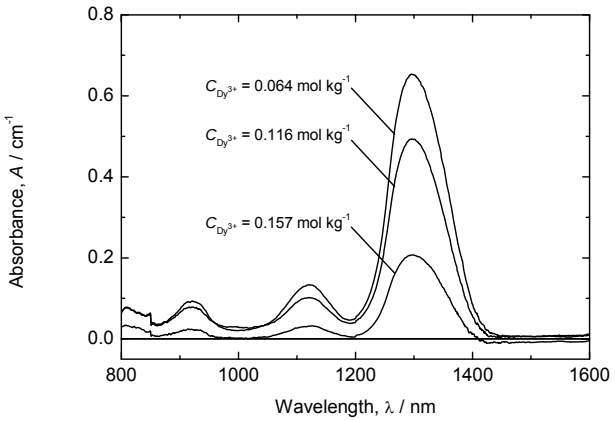

Fig. 1. Flowchart of the recycling process for neodymium magnet proposed in this study.

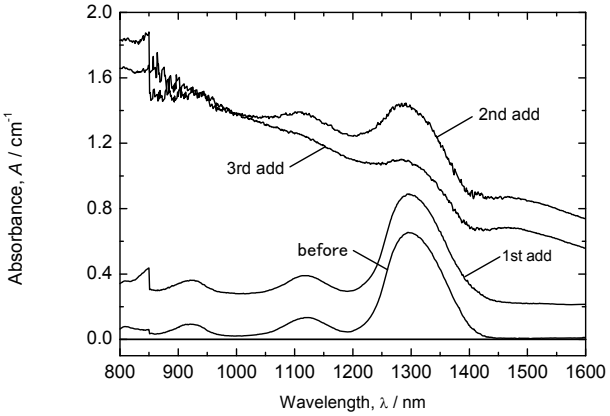

Fig. 2. Cyclic voltammogram of $CaCl_2$ molten salt and $CaCl_2$-Nd_2O_3-B_2O_3.

REFERENCES

H. Sekimoto, A. Uehara, T. Fujii, H. Yamana, KURRI Progress report, (2012) 102

採択課題番号 26P11-12　　吸光分光測定を用いた高温融体中の金属イオンの溶存形態に関する研究　（f-元素の有効利用に関わる基礎及び応用研究）プロジェクト

（岩手大・工）関本　英弘
（京大・原子炉）上原　章寛、藤井　俊行、山名　元

PR11-12 Elucidation of the Uptake Route of Radionuclides in Deciduous and Coniferous Trees Using Radio Cesium and Radio Potassium in Annual Tree Rings

T. Ohta, T. Kubota[1], Y. Shibahara[1], S. Fukutani[1] , T. Fujii[1]
T. Igarashi, Y. Mahara[2]

Faculty of Engineering, Hokkaido University
[1] Research Reactor Institute, Kyoto University
[2]Professor Emeritus, Kyoto University

INTRODUCTION:

Although previous studies have measured the distribution of radionuclides in tree rings, the uptake route of ^{137}Cs originating from the fallouts of nuclear weapon tests and the Chernobyl accident has undoubtedly argued the roots[1)-4)]. A number of researchers have also reported that ^{137}Cs and Pu are absorbed by trees through their bark and leaves; although ambiguously, conclusive evidence has been presented[5)].

Understanding the uptake route of radiocesium (radio-Cs) in the annual tree rings is important for a forest decontaminating in Fukushima. Thus, we investigated the fate of radio-Cs in the Fukushima forestry environment to understand its uptake route using following method: the behavior of radiocesium in the soil and the measurements of radiocesium in the annual tree rings of the deciduous tree konara and the coniferous tree sugi by gamma-ray spectrometry.

EXPERIMENTS

Our experiment is composed three objectives: 1) depth profile of ^{137}Cs, ^{134}Cs, and ^{40}K in the observed sites, 2) speciation of radio-Cs in soil, 3) measurement of ^{137}Cs and ^{40}K in tree rings

RESULTS:

The behavior of ^{137}Cs in the soil samples collected in Fukushima showed the following: (1) radio-Cs in the soil was primarily absorbed by soil minerals within the top 1-cm-depth from the surface; and (2) ^{137}Cs in soil was water insoluble and >95% of ^{137}Cs was bound to organic and residual matters. These observations suggest that the ^{137}Cs released from the Fukushima NPP was trapped in the surface soil and did not penetrate deeper into the soil. The results clearly show that radio-Cs in soil has not moved from the tree roots to the annual tree rings because the active root system rarely was found in the surrounding surface soil. The high ^{137}Cs concentration in the sapwood zone of konara coincided with the direction of the arriving radioactive plume in the sampling sites. Conversely, the concentrations of ^{137}Cs and ^{134}Cs in the annual tree rings of sugi showed non-directionality. As the radioactive Cs moved from the leaves to the tree trunk, the directionality of radio-Cs in the annual tree rings was eventually disappeared. The results of the present study indicate that ^{134}Cs and ^{137}Cs, detected in the tree rings, from the Fukushima NPP were directly absorbed from the atmosphere by the bark and leaves rather than the roots. Furthermore, the results suggest that the concentrations of radio-Cs in the trees in Fukushima would not further increase in the future.

On the basis of the distribution of radio-Cs in the annual tree rings of the both trees of konara and sugi, we propose the following guidelines for using contaminated wood from Fukushima when high concentrations ^{137}Cs have been detected in the trunk: (1) use the parts of wood where the ^{137}Cs concentrations are low, and (2) use the highest parts of the trees as sources of bio-ethanol and/or biomass, which correspond to the energy sources for the next generation.

REFERENCES:

[1] Fesenko et al., *Radiat. Environ. Biophys.*, **40**, 105 (2001).
[2]Goor and Thirty, *Sci. Total Environ*., **325**, 163 (2004).
[3] Momoshima et al., *J. Environ. Radioact.*, **22**, 93 (1994).
[4]Kagawa et al., *J. Environ. Qual.,* **31**, 2001 (2002).
[5]Kudo et al., J. Environ. Radioactivity, **21**, 55 (1993).

採択課題番号 26P11-13　福島の森林資源有効活用のための樹木年輪放射性核種の　プロジェクト取り込み経路の解明
（北大・工）太田朋子、五十嵐敏文（京大・原子炉）窪田　卓見、芝原雄司、福谷　哲、藤井俊行
（京都大学）馬原保典

PR11-13 Photon Activation Analysis of Alkali Earth Elements and Arsenic with Bremsstrahlung at the KURRI-LINAC

T. Kubota, T. Fujii, S. Fukutani, Y. Shibahara and T. Ohta[1]

Kyoto University Research Reactor Institute
[1]Graduate School of Engineering, Hokkaido University

INTRODUCTION: Photonuclear reaction induced by high energy photons can produce nuclides that are hardly produced in a nuclear reactor, for example, neutron deficient nuclides and carrier free isotopes through (γ, n) and (γ, p) reaction, respectively. High energy photon is generated in the bombardment of electrons of 30 MeV to platinum sheets at the KURRI-LINAC. We attempted to conduct activation analysis for silicate salt in the previous report [1]. However, Al-29 expected in (γ, p) reaction was not observed. The results showed the investigation of effective reaction cross-sections was required for various kinds of target samples. In this report alkali earth elements are used as target sample in order to obtain carrier free alkali metal elements, and in addition the concentration of arsenic in seaweed is evaluated as a preliminary test instead of neutron activation [2].

EXPERIMENTS: The target samples were once heated to dehydration and disintegrate organic compounds; alkali earth salts were dried at 100ºC; and seaweed (Hizikia fusiformis) was incinerated at 450ºC. Each sample was encapsulated in a quartz tube [3]. The tube in an aluminum vessel was irradiated with photon generated by electron energy of 30 MeV at average current of 200 μA for 4 to 48 hours. Radioactivity, A, induced by photonuclear reaction was measured by γ -spectrometry and provided the apparent cross-section, θ, which is determined by the following equation:

$$A = M_0\theta(\mu\mathrm{A})\left(1-e^{-\lambda t}\right)$$

where M_0, (μA), λ and t were mole number of target nuclide, average electron beam current (micro-ampere), decay constant, and irradiation time, respectively.

RESULTS: Fig 1 shows the apparent cross-sections as a function of mass number. The cross-section of (γ, n) reaction was larger than that of (γ, p) reaction by one order of magnitude. While the former was the largest at heavy element, seems to be constant between mass number of 40 to 100. The latter was almost constant independent of mass number. For a light element (γ, np) reaction was also observed; however, its cross-section was small. The measurement of activated seaweed shows the peaks of As-74 in Fig. 2. The cross-sections of some photonuclear reactions were obtained for isotope production and activate analysis, even though these values are empirical.

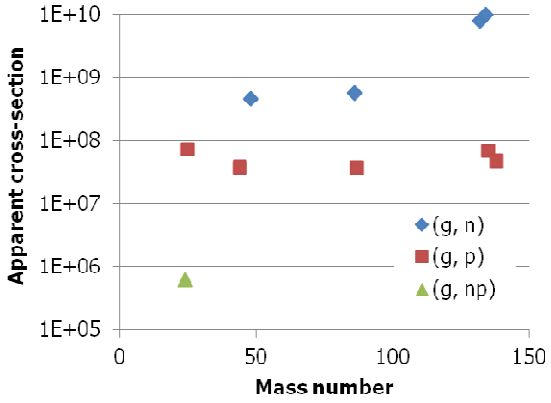

Fig. 1. Apparent cross-section for photonuclear reactions; (γ, n), (γ, p) and (γ, np) reaction

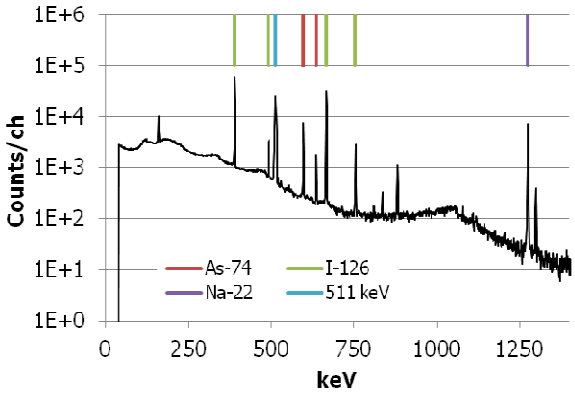

Fig. 2. Gamma spectrometry of seaweed (Hizikia fusiformis) irradiated for four hours at the KURRI-LINAC.

REFERENCES:

[1] T. Kubota et al., KURRI PROGRESS REPORT 2013 (2014) CO12-5.
[2] R. Ogawa et al., Bulletin of the Faculty of Education, Ehime University 53 (2006) 131-136.
[3] T. Kubota et al., Recent Advances in Actinide Science, RSC Publishing (2006) 68-70

採択課題番号 26P11-14　　海水中の放射性核種および重金属の濃度測定　　プロジェクト
（京大・原子炉）窪田卓見、藤井俊行、福谷　哲、芝原雄司（北大・工）太田朋子

PR11-14 Study of Applicability of Isotopic Ratio Measurement for Analysis of Radionuclide in Environmental Samples

Y. Shibahara, T. Kubota, S. Fukutani, T. Fujii,
T. Shibata[1], M. Yoshikawa[1]

Kyoto University Research Reactor Institute
[1] Kyoto University Institute for Geothermal Sciences

INTRODUCTION: For the analysis of radionuclide, the radiation measurement such as γ-spectrometry, β-spectrometry, and α-spectrometry were mainly performed. Although these methods have been used for the measurement of radioactive nuclide such as nuclear fuel materials and fission products released on the accident of Fukushima Dai-ichi Nuclear Power Plant, they may have disadvantage in the case of the analysis of radionuclide having the long half-life and/or that of isotopic composition including naturally occurring isotopes. Because the mass spectrometry has advantage for the analysis of the isotopic composition of the elements with high accuracy, this method may have the applicability for the analysis of radionuclide released on the accident of Fukushima Dai-ichi Nuclear Power Plant.

Although the amounts of radionuclide such as radioactive Cs and Sr released on this accident were very huge, the contaminated environmental samples show the small radioactivity per unit weight of the contaminated environmental samples, since the contaminated area is very wide. For the study of the recovery/analysis method of cesium and strontium, thus, the radioactive Cs and Sr were generated by the irradiation of natural uranium at KUR.

EXPERIMENTS: Radioactive Cs and Sr were generated by the irradiation of 10 mg of UO_2 of natural uranium at the Kyoto University Research Reactor with the neutron flux for 5.5×10^{12} n/s cm^2. The amounts of the major radionuclide of Cs and Sr generated by the irradiation for 3 hours were estimated as 7.4×10^{-11} g (^{137}Cs) and 4.5×10^{-11} g (^{90}Sr). About 2 days later, the irradiated sample was dissolved with 8M HNO_3 and heated to dryness. The residues were immersed in 8 M HNO_3 and the insoluble residues were removed by centrifugation. TRU elements in sample solution were removed by the extraction-chromatography with UTEVA-resin [1], and the sample solution was evaporated to dryness. The residues was dissolved with 3 M HNO_3 solution. After the recovery of Sr by the extraction-chromatography with Sr-resin [2], Cs was recovered by using with ammonium phosphomolybdate (AMP) [3]. The sample solutions for the analysis of isotopic composition of Sr and Cs were obtained with the dissolving 1 M HNO_3 (10μL for Sr, 20 μL for Cs, respectively).

Isotopic compositions of Cs and Sr were measured with a TIMS (Triton-T1, Thermo Fisher Scientific). A 1 μL aliquot of each solution was loaded onto a rhenium single filament with a TaO activator [4]. Loading amount of ^{90}Sr and ^{137}Cs were 4.5×10^{-12} g and 3.7×10^{-12} g, respectively. Because of the loading amount of Sr and Cs, the mass spectra of radioactive Cs and Sr were obtained with a secondary electron multiplier detector (SEM).

RESULTS: In the measurement of radioactive Cs, ^{135}Cs, ^{136}Cs and ^{137}Cs were detected (Fig.1 (a): ^{134}Cs was not detected, because of the amount generated by the irradiation at KUR. In this measurement, it was observed that the isotopic ratios of ^{135}Cs/^{137}Cs and ^{136}Cs/^{137}Cs were 0.9103±0.0008 and 0.00022±0.00001, respectively. These mean that the several ten femto-gram of Cs would be detectable with the four orders of the significant figures.

In the measurement of radioactive Sr, ^{89}Sr, ^{90}Sr and ^{91}Sr were detected at the measurement 2.6 days later. The mass spectra of ^{91}Sr and ^{89}Sr were disappeared at the measurement of 31 days later and 574 days later, because of the half-life of ^{91}Sr ($T_{1/2}$ = 9.5 h) and ^{89}Sr ($T_{1/2}$ = 50.5 d). The obtained isotopic ratios were agreed with results of the estimation by using ORIGEN-II code [5]. This means that the several ten femto-gram of Sr would also be detectable.

It was confirmed that the recovery/analysis method of Cs and Sr have the applicability for the analysis of radioactive Cs and Sr released on the accident of Fukushima Dai-ichi Nuclear Power Plant. The loading amount of several pico-grams of radioactive Cs and Sr would bring the information of the isotopic ratio with the four orders of significant figure until the ten periods of half-live.

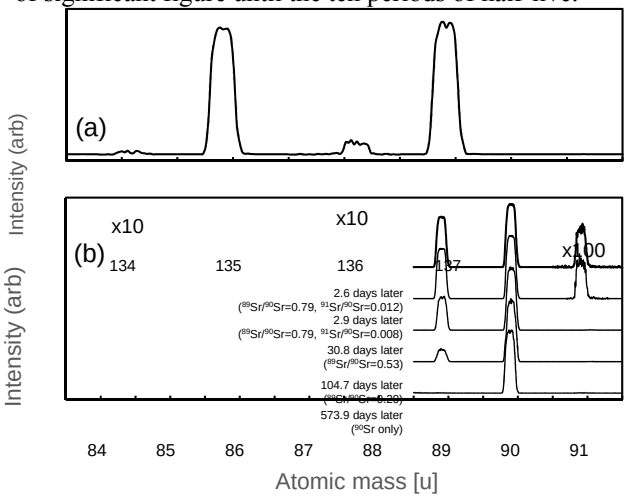

Fig.1 Mass spectra of radioactive Cs and Sr. (a) Cs, (b) Sr.

REFERENCES:

[1] Y. Shibahara et al., J. Radioanal. Nucl. Chem., 303: 1421-1424 (2015).
[2] T. Kubota et al., J. Radioanal. Nucl. Chem. 303: 39-46 (2015).
[3] Y. Shibahara et al., J. Nucl. Sci. Technol. 51: 575-579 (2014).
[4] J. L. Birck, Chem. Geol. 56: 73-83 (1986).

採択課題番号26P11-15 境試料中の放射性核種分析への同位体比分析法の適用の検討　プロジェクト（京大・原子炉）芝原雄司、窪田卓見、福谷哲、藤井俊行（京大・地熱研）柴田知之、芳川雅子

PR11-15 Tracing Halogen and Noble Gas Recycling in the Northern Izu Subduction Zone by Neutron Irradiation and Noble Gas Mass Spectrometry

H. Sumino, M. Kobayashi, K. Nagao, R. Okumura[1], S. Sekimoto[1] and T. Fujii[1]

Geochemical Research Center, Graduate School of Science, University of Tokyo
[1] Research Reactor Institute, Kyoto University

INTRODUCTION: Recent findings of subducted halogens and noble gases with seawater and sedimentary pore-fluid signatures in exhumed mantle wedge peridotites [1], as well as seawater-derived heavy noble gases (Ar, Kr, and Xe) in the convecting mantle [2], provide observations that allow us to investigate the processes that control the return of volatile and highly incompatible elements into the mantle. To verify whether and how such subduction fluids modify the composition of the mantle beneath subduction zones, we are investigating noble gas and halogen compositions of olivines in arc lavas from northern Izu subduction zone and those of seafloor sediments and basalts from NW margin of the Pacific plate. A combination of neutron irradiation and noble gas mass spectrometry (NI-NGMS), an extension of Ar-Ar and I-Xe dating methods, allows us to simultaneously determine trace amounts of halogens with naturally occurring noble gases by use of ultrahigh-sensitive noble gas mass spectrometry on neutron-irradiated samples [3,4].

EXPERIMENTS: The samples and standard samples for NI-NGMS, Hb3gr hornblende and the Shallowater meteorite were neutron-irradiated for six hours during a 5 MW operation of KUR by using the hydraulic conveyer to convert halogens (Cl, Br, and I) to corresponding noble gas isotopes. Noble gases in the unirradiated and irradiated samples were extracted selectively from fluid/melt inclusions using *in vacuo* crushing. The evolved noble gases were analyzed using mass spectrometry at The University of Tokyo [5,6].

RESULTS: MORB-like $^{3}He/^{4}He$ and halogen ratios of the olivines indicate insignificant contributions to the Izu arc magmas of radiogenic ^{4}He and sedimentary-pore-fluid-like halogens, both of which are observed in the subduction fluids released from a slab at a depth of 100 km [1]. On the other hand, a clear difference in $^{40}Ar/^{36}Ar$ ratios between the Izu volcanic front and rear arc, and a comparison with those of the seafloor sediments and altered oceanic crusts suggest that Ar of sedimentary pore-water origin in the subducting slab or hydrated layer of the mantle wedge is liberated continuously with depth and that it affects the noble gas composition of the magma generation region significantly. A small addition of the sediment-derived noble gases to the rear-arc magma is consistent with the slab melt contribution inferred from trace element and Pb-Sr-Nd-Hf) isotope compositions [7].

The high I/Cl ratios of the seafloor sediments can account for the enrichment of I in subduction fluids relative to sedimentary pore-fluids [1], whereas contributions of halogens and noble gases from altered oceanic basalts are limited.

A simple mass balance calculation of Ar isotopes for the melt generation region beneath the Izu arc revealed that higher subduction flux of pore water other than direct incorporation with its host sediment/crust is necessary, and that serpentinized lithosphere in the subducting slab is regarded as the best candidate if the hydration of the lithosphere by pore fluids is operating in a closed system.

The significantly smaller contributions of subducted noble gases and halogens in the Izu arc magmas relative to those in the mantle wedge peridotites may result from a difference in the P-T condition of the slab in each subduction zone, or from dilution by mantle-derived halogens and He when the subduction fluid induced partial melting. The former implies a relatively small amount of the pore-water-derived subduction fluids would be released from a cold slab at a sub-arc depth resulting in further subduction of halogens, heavy noble gases and potentially water, to great depths in the mantle, which account for the seawater-like heavy noble gases observed in the convecting mantle [2].

REFERENCES:

[1] H. Sumino *et al.*, Earth Planet. Sci. Lett., **294** (2010) 163-172.
[2] G. Holland and C.J. Ballentine, Nature, **441** (2006) 186-191.
[3] G. Turner, J. Geophys. Res., **70** (1965) 5433-5445.
[4] J.K. Böhlke and J.J. Irwin, Geochim. Cosmochim. Acta, **56** (1992) 187-201.
[5] N. Ebisawa *et al.*, J. Mass Spectrom. Soc. Jpn., **52** (2004) 219-229.
[6] H. Sumino *et al.*, J. Mass Spectrom. Soc. Jpn., **49** (2001), 61-68.
[7] J.-I. Kimura *et al.*, Geochem. Geophys. Geosys., **11** (2010) Q10011.

採択課題番号 26P11-16　希ガス化法を用いた極微量ハロゲン測定による地球深部の水の起源の解明　　プロジェクト

（東大院・理・地殻化学実験施設）角野浩史、長尾敬介、小林真大
（京大・原子炉）藤井俊行、関本 俊、奥村 良

PR11-16 Volcanic and Tectonic History of Philippine Sea Plate (South of Japan) Revealed by $^{40}Ar/^{39}Ar$ Dating Technique

O. Ishizuka, T. Fujii[1], R. Okumura[1], S. Sekimoto[1]

Geological Survey of Japan, AIST
[1]Research Reactor Institute, Kyoto University

INTRODUCTION: Submarine volcanic rocks are known to give ages different from their true eruption ages in some cases. This is due to the existence of excess ^{40}Ar in the rapidly quenched glass or Ar loss and K remobilization caused by reaction with seawater or hydrothermal fluids. Stepwise-heating analysis in $^{40}Ar/^{39}Ar$ dating is particularly useful for dating submarine volcanics.

Since this is the first time to use KUR for our laboratory, we investigated neutron flux gradient and production of interfering isotopes for $^{40}Ar/^{39}Ar$ method by irradiating standard minerals and synthetic glasses as preparation for dating of unknown samples.

EXPERIMENTS: Samples were wrapped in an aluminum foil packet and the packets were piled up in a pure aluminum (99.5% Al) irradiation capsule (9 mm diameter and 30 mm long). The irradiation capsule was partitioned into 3 compartments to minimize the uncertainty of the sample positions at irradiation. The irradiation capsule was wrapped with 0.5 mm-thick Cd-foil before irradiation. The capsule was irradiated 2 hours at 5MW in Hyd facility of KUR. Analyses were conducted using $^{40}Ar/^{39}Ar$ geochronology facility at the Geological Survey of Japan/AIST following the analytical procedure described in [1].

For the experiments described here, around 15 mg of sample was analyzed in each analysis. Due to alteration of poorly-crystallized part groundmass, basaltic samples were treated at 100°C on hot plate with stirrer in 6N HCl for 60 minutes and then 6N HNO_3 for 60 minutes to remove possible alteration products (clays and carbonates) prior to irradiation. This procedure effectively separated and concentrated fresh plagioclase in groundmass and of microphenocryst. After this acid treatment, these separates were examined under binocular microscope before packed for irradiation.

RESULTS: Two basaltic samples recovered from the northern margin of the Palau Basin, southernmost part of the Philippine Sea plate, were studied. The West Philippine Basin and Palau Basin are supposed to have been the oldest oceanic basins in the Philippine Sea Plate. Accordingly, their origin and growth history can be a critical constraint on the tectonic reconstruction of the Philippine Sea Plate. These basins could have existed prior to the Izu-Bonin (Ogasawara)-Mariana arc (IBM arc), or formed as a consequence of subduction initiation along the IBM arc (e.g., backarc basins of the IBM arc). However, due to the paucity of geological and geophysical data from these basins, their origin and history are yet unclear.

YK10-14 and YK13-08 cruises by R/V Yokosuka investigated Palau Basin) and southern part of West Philippine Basin obtained crucial geological and geophysical data [2] for reconstruction of the Philippine Sea Plate. 12 dredge hauls and 4 Shinkai submersible dives were made during these cruises. $^{40}Ar/^{39}Ar$ dating of dolerite sample from the Palau Basin crust exposed at the Mindanao Fracture Zone at c. 130°E gave a plateau age of 40.4 Ma. This result implies that the spreading of the Palau Basin was still going on at 40.4 Ma. This age is within an age range of active spreading of the West Philippine Basin.

This year we conducted $^{40}Ar/^{39}Ar$ dating of basaltic samples from 2 locations in the eastern part of the basin along the Mindanao Fracture zone. Fig. 1 shows age spectra for the 2 analyses. Sample 6K1358R11, which was collected by Shinkai 6500 at 4564 m deep gave a plateau age comprising of 63.8% of released gas. YK10-14 D3R14, which was collected further east along the Mindanao Fracture Zone by dredging also gave a well-defined plateau comprising of 96.3% of released gas. The plateau ages shown here are still temporary age because flux monitor measurement has not been completed yet. However, these data strong imply that the age of formation of the Palau Basin closely matches with that of West Philippine Basin, and this result is crucial for tectonic reconstruction of this area. Final ages will also allow us to determine the direction and rate of seafloor spreading when the Palau Basin formed.

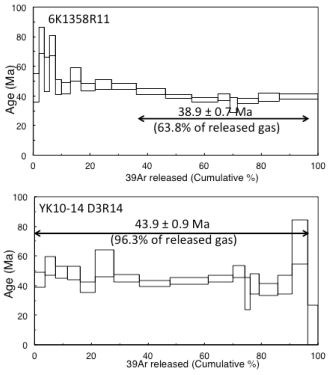

Fig. 1 Age spectra for the basalts from the Palau Basin.

REFERENCE:

[1] O. Ishizuka *et al.*, Chem. Geol., **266** (2009), 274-296.
[2] Sasaki, T., Yamazaki, T., Ishizuka, O., (2014) Earth Planet. Space, 66:83, doi:10.1186/1880-5981-66-83.

採択課題番号 26P11-17　$^{40}Ar/^{39}Ar$ 年代測定による日本周辺海域の火山活動史及び地殻構造発達史の解明　プロジェクト

（産総研）石塚　治（京大・原子炉）藤井　俊行、奥村 良、関本　俊

PR11-17 Ar–Ar Age Determination of Minamitorishima

N. Hirano, H. Sumino[1], T. Fujii[2], R. Okumura[2], S. Sekimoto[2]

Center for Northeast Asian Studies, Tohoku University
[1] Geochemical Research Center, Tokyo University
[2] Research Reactor Institute, Kyoto University

INTRODUCTION: Most of seamounts on the western Pacific Plate formed before 70 Ma in the so-called West Pacific Seamount Province (WPSP) which is characterized by relatively short seamount chains maybe indicating a significant short-lived hotspot system [1]. The geochronological studies of each Cretaceous seamount, on the other hand, show the long-lived main shield stage of volcanism, because a seamount remained above a hotspot for a long time (approximately 10 m.y. [2]). This may be attributed to either of the following two possibilities: 1) An abundant heat supply as in the superplume episode in the Early Cretaceous [3][4][5]. 2) Slow absolute motion of the Early Cretaceous Pacific Plate (3–6 cm/yr.) [6][7].

The research cruise using R/V *Yokosuka* equipped with the submersible *SHINKAI 6500*, was conducted around the Minamitorishima Island on May 2010 in order to know the detail history during the formation of the island, where volcanic rock samples have never been obtained before (Fig. 1). The shipboard multibeam acoustic surveys showing the detail bathymetry discovered the volcanic cones on seamount slope and the clusters of small conical volcanoes on surrounding abyssal plain (Oikawa and Morishita, 2009). Most of cones are several hundred meters in height and 1–10 km in diameter. We observed the stratigraphy of Minamitorishima using the submersible *SHINKAI 6500*. Highly vesicular lavas were sampled at the volcanic cone on the seamount slope. The olivine-bearing dense lavas, on the other hand, were obtained at the steep slope beneath the lava platform in bathymetry, implying main-shield stage lavas in contrast to volcanic cones probably erupted at the rejuvenated stage during the Minamitorishima's formation.

EXPERIMENTS: Radiometric Ar-Ar dating is commonly used to determine the ages of submarine lavas, because the traditional K-Ar dating is impossible to remove the alteration part in such rocks [8]. The rock-samples prepared for dating were crushed to 100-500 μm grains, and leached by the 1N HNO_3 at 70-60 °C for one hour. The leached samples were irradiated by neutrons in a reactor to produce ^{39}Ar from ^{39}K during a few hours. During the irradiation, samples were packed with EB-1 biotite flux monitors [9], K_2SO_4 and CaF_2 as correcting factors in an aluminum capsule. They are shielded by Cd foil in order to reduce neutron-induced ^{40}Ar from ^{40}K [10]. Then, radiogenic ^{40}Ar, daughter nuclide of radioactive ^{40}K and parent, ^{39}Ar instead of ^{40}K, were simultaneously analyzed using a mass-spectrometer with an extraction technique of multi-step heating of approximately every 50 to 100 °C between 500 to 1500 °C.

RESULTS: The irradiations of sample in KUR were done in May, 2014. We are going to analyze the irradiated samples after cooling. We note that the Minamitorishima is just only "island" in WPSP in spite of many of larger volcanic edifices of seamount and guyot than Minamitorishima. We have a hypothesis of different process and age to make the island in WPSP, awaiting future analytical results

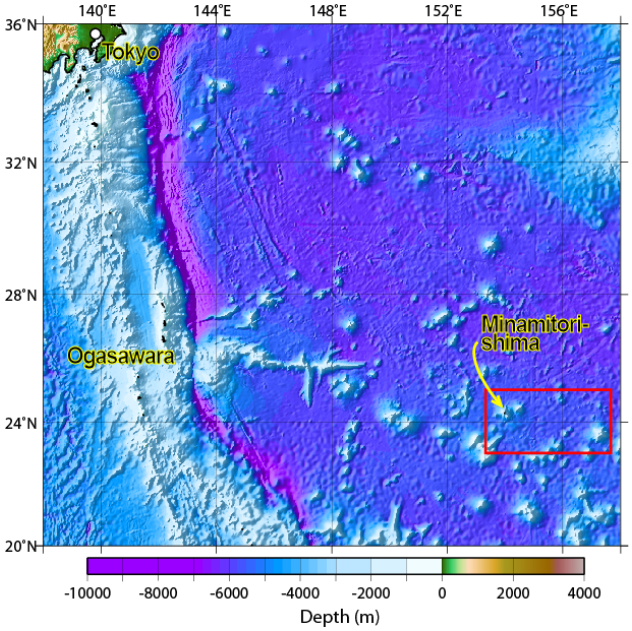

Fig. 1. Bathymetric map of Western Pacific.

REFERENCES:

[1] A. A. P. Koppers *et al.*, *Geochem. Geophys. Geosyst.*, **4** (2003) DOI | 10.1029/2003GC000533
[2] N. Hirano *et al.*, *Marine Geol.*, **189** (2002) 371-379.
[3] K. G. Cox, *Nature*, **352** (1991) 564-565.
[4] R. L. Larson, *Geology*, **19** (1991) 547-550.
[5] R. L. Larson and C. Kincaid, *Geology*, **24** (1996) 551-554.
[6] R. A. Duncan and D. A. Clague, in *The ocean basins and margins*, 89-121 (New York, Plenum, 1985)
[7] J. W. Henderson *et al.*, *Tectonics*, **3** (1984) 121-132.
[8] I. McDougall and T. M. Harrison, in *Geochronology and Thermochronology by the $^{40}Ar/^{39}Ar$ Method*, (Oxford, New York, 1988).
[9] N. Iwata, Ph.D. Thesis, Tokyo Univ. (1998).
[10] K. Saito, *Sci. Rep. Res. Inst. Tohoku Univ. (RITU), Japan* **A40** (1994) 185-189.

採択課題番号 26P11-18　新種の火山のメカニズムを解明するための $^{40}Ar/^{39}Ar$ 年代測定 プロジェクト（京大・原子炉）藤井俊行、関本俊、奥村良（東大院・理・地殻化学実験施設）角野浩史、（東北大・東北アジア研究センター）平野直人